ACS APPLIED MATERIALS & INTERFACES

Research Article

www.acsami.org

Facile Fabrication of Superhydrophobic Surface with Excellent Mechanical Abrasion and Corrosion Resistance on Copper Substrate by a Novel Method

Fenghua Su* and Kai Yao

School of Mechanical and Automotive Engineering, South China University of Technology, Guangzhou 510640, P. R. China

Web-Enhanced Feature

ABSTRACT: A novel method for controllable fabrication of a superhydrophobic surface with a water contact angle of 162 ± 1° and a sliding angle of 3 ± 0.5° on copper substrate is reported in this Research Article. The facile and low-cost fabrication process is composed from the electrodeposition in traditional Watts bath and the heat-treatment in the presence of (heptadecafluoro-1,1,2,2-tetradecyl) triethoxysilane (AC-FAS). The superhydrophobicity of the fabricated surface results from its pine-cone-like hierarchical micro-nanostructure and the assembly of low-surface-energy fluorinated components on it. The superhydrophobic surface exhibits high microhardness and excellent mechanical abrasion resistance because it maintains superhydrophobicity after mechanical abrasion against 800 grit SiC sandpaper for 1.0 m at the applied pressure of 4.80 kPa. Moreover, the superhydrophobic surface has good chemical stability in both acidic and alkaline environments. The potentiodynamic polarization and electrochemical impedance spectroscopy test shows that the as-prepared superhydrophobic surface has excellent corrosion resistance that can provide effective protection for the bare Cu substrate. In addition, the as-prepared superhydrophobic surface has self-cleaning ability. It is believed that the facile and low-cost method offer an effective strategy and promising industrial applications for fabricating superhydrophobic surfaces on various metallic materials.

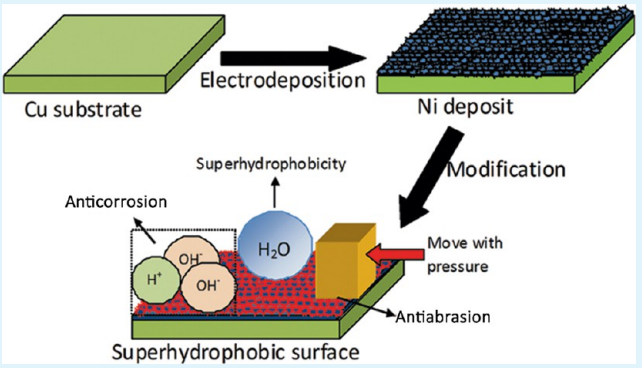

KEYWORDS: *superhydrophobic surface, mechanical stability, anticorrosion, self-cleaning*

1. INTRODUCTION

Superhydrophobic surfaces with a contact angle greater than 150° and a sliding angle less than 10° attracted tremendous attention for researchers because of its great importance in fundamental research, as well as its potential in industrial use. These superhydrophobic surfaces have many practical applications in various areas, such as self-cleaning,[1] anticorrosion,[2,3] anti-icing,[4] oil−water separation,[5,6] and microfluidic devices.[7] The key element to construct superhydrophobic surface is the presence of a low energy hydrophobic surface coating on a rough structure with special micro-nanostructures.[8−13] Up to know, a great number of methods have successfully constructed superhydrophobic surfaces, such as chemical vapor deposition,[14] chemical etching,[15] sol−gel technique,[16] solution-immersion method,[17] spin coating,[9] and laser fabrication.[18] However, some of the fabrication techniques for making superhydrophobic surfaces are potentially costly and time-consuming for practical implementation in applications. Because of the facile, low cost and suitable for industrial applications, electrodeposition is thought to be an effective technique for constructing large-area superhydrophobic surface.[10,19]

The scientific and engineering value of superhydrophobic surface is dramatically limited as it has weak mechanical abrasion resistance. As mentioned above, although different superhydrophobic surfaces have been constructed by various techniques, few coatings were reported to be actually used in industrial applications because of their poor mechanical abrasion resistance and surface chemical stability. Some superhydrophobic surfaces are even fragile to the finger contact. Obviously, the acquiring of excellent mechanical abrasion resistance and chemical stability for superhydrophobic surface is an urgent demand for their practical applications. Recently, a few reports investigated the mechanical stability,[13,20−22] chemical stability,[23,24] and long-term stability[25] of the as-constructed superhydrophobic surface. Zhu et al.[20,21] evaluated the mechanical stability of the prepared superhydrophobic metal/polymer composite and fabric surfaces by a simple finger pressing and scratch test. Unfortunately, few work systemically evaluated the mechanical abrasion resistance of superhydrophobic surfaces.[3,26] She et al.[3] prepared a robust and

Received: March 15, 2014
Accepted: April 25, 2014
Published: April 25, 2014

ACS Publications © 2014 American Chemical Society

dx.doi.org/10.1021/am501539b | ACS Appl. Mater. Interfaces 2014, 6, 8762−8770

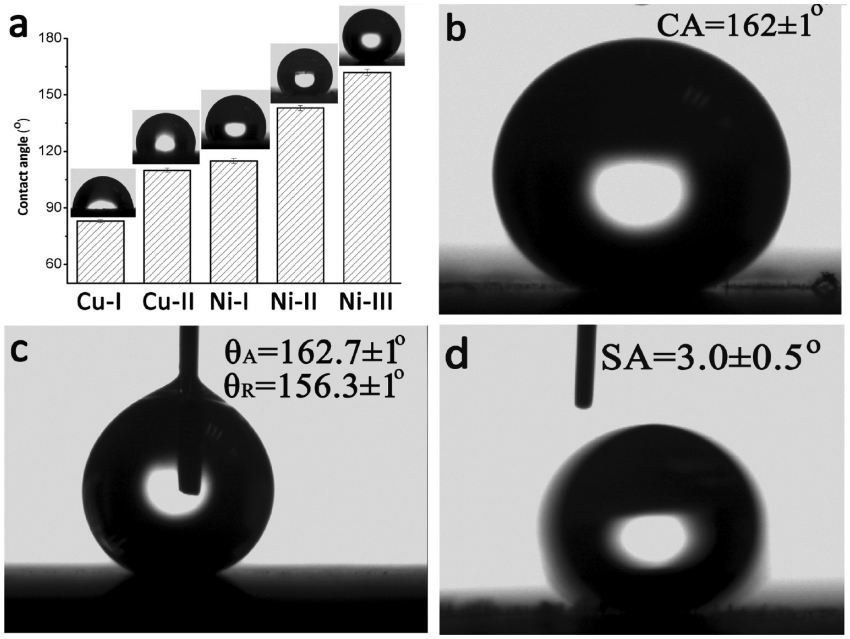

Figure 1. (a) Comparisons of the contact angle of water droplet on various sample surfaces. (b) Contact angle of a water droplet on the superhydrophobic surface (Ni-III). (c) Advancing/receding contact angle (θ_A/θ_R) of a water droplet on the superhydrophobic surface. (d) Water droplet rolling down the superhydrophobic surface and its sliding angle.

stable superhydrophobic surface on magnesium alloy substrate. With the SiC sandpaper (800 mesh) was served as an abrasion surface, the as-prepared surface still maintained the contact angle above 150° after mechanical abrasion for 0.7 m under a pressure of 1.2 kPa.

Copper (Cu) and its alloys is one of the important materials in industry owing to its high electrical and thermal conductivities, mechanical workability and relatively noble properties. It is widely used in many applications such as a conductor in electrical power lines and pipelines, heat conductors and heat exchangers. One of the major challenges in Cu applications is the prevention of Cu corrosion, which leads to inferior device performance and failure. In the recent years, research was carried out to construct superhydrophobic surface on Cu substrate to improve its corrosion resistance.[27,28] Liu et al.[27] found the constructed superhydrophobic surface significantly improved the corrosion resistance of Cu in seawater. Yuan et al.[28] also constructed a superhydrophobic fluoropolymer films on Cu substrate to improve its corrosion resistance. However, the mechanical abrasion resistance of the superhydrophobic surfaces on Cu substrate was not reported in these literatures.

From the above analysis, it can be seen that excellent mechanical abrasion and corrosion resistance is very important for the constructed superhydrophobic surfaces on metal substrates for their wide applications. In this work, a facile and low-cost method is used to produce a superhydrophobic surface on Cu substrate. The fabrication process is composed from two steps: the electrodeposition in traditional Watts bath and the heat-treatment in the presence of AC-FAS. The as-prepared surface displays superhydrophobicity with a water contact angle around 162° and a water sliding angle around 3°. Additionally, the as-prepared superhydrophobic surface has excellent mechanical abrasion resistance, excellent corrosion resistance and self-cleaning properties, which removes the major barriers to its practical applications.

2. EXPERIMENTAL SECTION

2.1. Materials. Nickel sulfate ($NiSO_4$), nickel chloride hexahydrate ($NiCl_2{\cdot}6H_2O$), and boric acid (H_3BO_3) were supplied by Guangzhou Chemical Reagent Factory, China. (Heptadecafluoro-1, 1, 2, 2-tetradecyl) triethoxysilane ($CF_3(CF_2)_7(CH_2)_2Si(OC_2H_5)_3$, AC-FAS) was supplied Guangzhou Liyuan Chemical Materials Co., China. Anhydrous ethanol was provided by Guangzhou Donghong Chemical Plant, China. All chemical reagents are analytical and used without further purification.

2.2. Sample Preparation. The nickel (Ni) electrodeposit were obtained in traditional Watts bath containing $NiSO_4$ (320 $g{\cdot}L^{-1}$), $NiCl_2{\cdot}6H_2O$ (50 $g{\cdot}L^{-1}$), and H_3BO_3 (450 $g{\cdot}L^{-1}$). A copper plate with a size of 40× 20 ×1 mm was used as the working cathode. Prior to plating, it was mechanically polished to a 0.06−0.10 μm surface finish, and cleaned ultrasonically with distilled water and acetone to remove contamination on the substrate surface. The platinum mesh with the dimension of Ø 50.0 mm was used as anode. The electrodeposition was conducted with a direct current density of 0.75 $A{\cdot}cm^{-2}$ at 50 °C for 1 h. After deposition, the Ni deposit was rinsed with distilled water and dried at 80 °C for 2 h. The Ni deposit and the bare Cu substrate were abridged as Ni−I and Cu−I, respectively.

In the next step, the as-prepared deposit was put into a sealed reactor, which contained 10 mL 5 wt. % AC-FAS ethanol solution, and heat-treated at 110 °C for 1 h in an oven. After heat-treatment, the samples was rinsed with distilled water and dried with hairdryer to obtain the superhydrophobic surface. For comparison, the Ni deposit was also heat-treated at 110 °C for 1 h in an oven but in the absence of AC-FAS ethanol solution. Ni-II will be heat treated without AC-FAS and Ni-III will be heat treated with AC-FAS as described in the following section. The Cu substrate was also treated with the same method of Ni-III for reference, which was abridged as Cu−II.

2.3. Characterizations. The water contact angle and sliding angle were measured with approximately 5 μL water droplets using a measuring apparatus (Dataphysics OCA40 Micro) at ambient temperature. The values reported are the average of five measurements made on different positions of the sample surface. Surface morphologies of various samples were studied using a field emission scanning electron microscope (FESEM, Nova NanoSEM 430). The chemical compositions of the samples were investigated with a Fourier-transform infrared spectrophotometer (FTIR, Bruker Vector

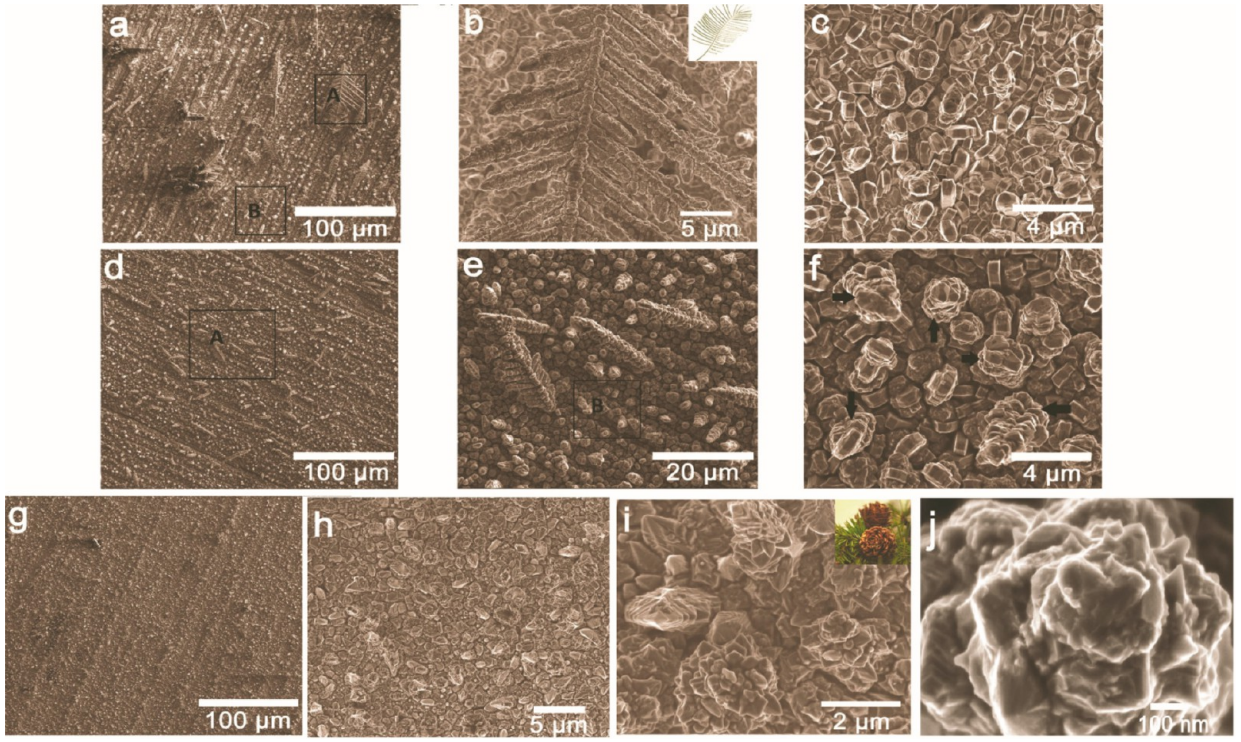

Figure 2. SEM and FE-SEM images of deposited Ni (Ni-I), hydrophobic Ni (Ni-II), and superhydrophobic Ni (Ni-III) surfaces: (a) Ni−I, (b) enlarged zone of A in panel a (inset, a photograph of needle-like leaf), (c) enlarged zone of B in panel a, (d) Ni-II, (e) enlarged zone of A in panel d, (f) enlarged zone of B in panel e, (g) superhydrophobic surface, (h) high magnification of panel g, (i) high magnification of h (inset, a photograph of a pine cone), and (j) FE-SEM image of a pine-cone structure.

33) and X-ray photoelectron spectrometer (XPS, Kratos Axis Ultra DLD). The sample surface roughness was characterized with a BMT Expert 3D surface profile measurement system. The mechanical stability of the obtained samples was evaluated by scratch test, microhardness test, and pencil hardness test. The scratch test was carried out on a homemade scratch tester with 800 grit SiC sandpaper as an abrasion surface. The sample surfaces were tested facing this abrasion surface with varying applied load and distance. The microhardness of samples was measured on a Vickers microhardness tester with a load of 100 g applied for 15 s. The pencil hardness tests for the coatings are carried out according to the standard of ASTM D3363-05. It uses pencil leads of different hardness grades (6B-6H).

Electrochemical corrosion test was carried out in a three electrode cell. A platinum plate and saturated calomel electrode (SCE) were used as the counter and reference electrode, respectively. The as-prepared deposit was used as a working electrode. Measurements were performed in 3.5 wt % NaCl solution by an electrochemical workstation (CorrTest CS310, Wuhan Corr Test Instrument Co. Ltd., China) at room temperature. Before the electrochemical tests, coatings were mounted using paraffin wax with a surface area of 1 cm^2 exposed to the corrosive medium. The potentiodynamic anodic polarization curves were recorded at a sweep rate of 0.5 $mV{\cdot}s^{-1}$ from −250 to 250 mV versus the open circuit potential. The corrosion potential (E_{corr}), corrosion current density (I_{corr}) and corrosion rate were determined using the Tafel extrapolation from the polarization curves. As to electrochemical impedance spectroscopy (EIS) measurements, the employed amplitude of the sinusoidal signal was 10 mV, and the frequency range studied was from 10^5 to 10^{-2} Hz. The average value from four replicates for each kind of specimen was reported.

3. RESULTS AND DISCUSSION

3.1. Wettability, Morphology, and Chemical Compositions. Figure 1 a shows that the Cu substrate (Cu−I) is hydrophilcity due to its water contact angle around 83°. After heat-treatment at 110 °C for 1 h, the contact angle of Cu−II slightly increases to 110° although the AC-FAS was used during modification process. The contact angle of the deposited Ni (Ni−I) is around 115°, suggesting the simple electrodeposition process cannot achieve hydrophobicity on the surface. Interestingly, the contact angle of 143° is achieved for the Ni deposit (Ni-II) as it was heat-treated in the absence of AC-FAS. As the AC-FAS was added during the heat-treating process, the Ni deposit (Ni-III) obtains a contact angle around 162°, as shown in Figure 1a and b. The result shows that the superhydrophobic surface is achieved as the deposited surface was heat-treated in the presence of AC-FAS. Figure 1c shows that the superhydrophobic surface of Ni-III has an advancing contact angle (θ_A) of 162.7° and a receding contact angle of 156.3°, suggesting the as-prepared superhydrophobic surface having very low sliding angle. Figure 1d confirms that the water droplet on the superhydrophobic surface rolls off the nearly horizontal surface immediately without any adhesion, which agrees well with the advancing/receding contact angle in Figure 1c. The test results show the superhydrophobic surface has an ultra-low sliding angle around 3.0°, which means the as-prepared surface possesses excellent water repellent property. In addition, the dynamic behavior of water droplets was also investigated. It can be seen that water stream can bounce off from the superhydrophobic surface without leaving a trace (Video 1). The results suggest that the as-prepared superhydrophobic surface is very stable and has strong superhydrophobicity.

SEM images of the deposited Ni (Ni-I), hydrophobic Ni (N-II), and superhydrophobic Ni (Ni-III) surfaces are shown in Figure 2. As shown in Figure 2a, the morphology of the deposited Ni surface is composed from a few large dendrites, a few twig-like branches and a large number of microparticles.

The large dendrite contains many twig-like branches that are featured with a length ranging from a few micrometers to dozens of micrometers, as shown in Figure 2b. Figure 2c shows that microparticle is featured with an average diameter of 1−2 μm, cylindrical shape, and smooth surface. After heat treatment in the absence of AC-FAS, the hydrophobic Ni surface consists of more twig-like branches and a large number of microparticles but don't have any large dendrites (Figure 2d and e). Interestingly, the microparticle morphology in this surface is different from that in the Ni-I surface. Most of microparticles remain cylindrical, but a few microparticles have changed to be pine-cone-like structure, as marked with arrows in Figure 2f. The appeared pine-cone-like structure might correspond to the improved hydrophobicity for the heat-treated Ni (Ni-II) surface.

Surprisingly, after heat-treating in the presence of AC-FAS, the as-prepared superhydrophobic surface is covered with large amounts of smaller microparticles but don't have any dendrites and twig-like branches, as shown in Figure 2g. The size and the surface of the microparticles become smaller and rougher, respectively, as shown in Figure 2h. In addition, the microparticle morphology has changed to be pine-cone-like structure from cylindrical structure. Careful inspections of the superhydrophobic surface show that the microparticles are pine-cone-like microclusters with average diameter of 1−2 μm, as shown in Figure 2i. Figure 2j shows the FE-SEM image of the pine-cone-like structure in this superhydrophobic surface. It can be seen that the pine-cone-like microcluster consists of numerous irregular petal-like structures with size ranging from dozens to hundreds of nanometers, which suggests that the pine-cone-like microclusters are hierarchical micro-nanostructure. In general, these results from Figure 2 suggest the surface featured with pine-cone-like hierarchical micro-nanostructure favors the acquiring of the superhydrophobic surface. The pine-cone-like hierarchical structures can generate numerous grooves in which the air can be trapped that can lead to the larger contact angle and smaller sliding angle according to the Cassie−Baxter equation.[3,29]

Surface roughness profile curves are shown in Figure 3 to elaborate the relationships between the surface roughness and the wettability for these samples. The bare Cu substrate has a surface roughness around 0.08 μm. After heat-treatment in the presence of AC-FAS, its surface roughness slightly decreases to 0.06 μm. However, the surface roughness increases from 0.08 μm for the Cu substrate to 1.86 μm for the deposited Ni surface. After heating treatment, the surface roughness of the hydrophobic Ni-II decreases to 1.40 μm, which agrees well with the morphology shown in Figure 2 due to the disappearance of large dendrites. As expected, the superhydrophobic surface (Ni-III) displays a surface roughness of 1.18 μm, because it is only covered with smaller microparticles (Figure 2g). The results confirm that the deposited surfaces have much higher surface roughness than the bare Cu substrate, irrespectively of the subsequent modification process. As is well known, the rough surface is necessary for achieving a superhydrophobic surface. To obtain a superhydrophobic surface, the surface roughness must reach the Cassie-Baxter state.[30] But, the surface roughness is by no means the only factor to determine the superhydrophobicity of the surface. Although Ni-III displays lower surface roughness than Ni−I and Ni-II, it has superhydrophobicity with a contact angle of 162° and sliding angle of 3.0°. The superhydrophobicity of Ni-III surface results from its pine-cone-like hierarchical structures and its chemical compositions.

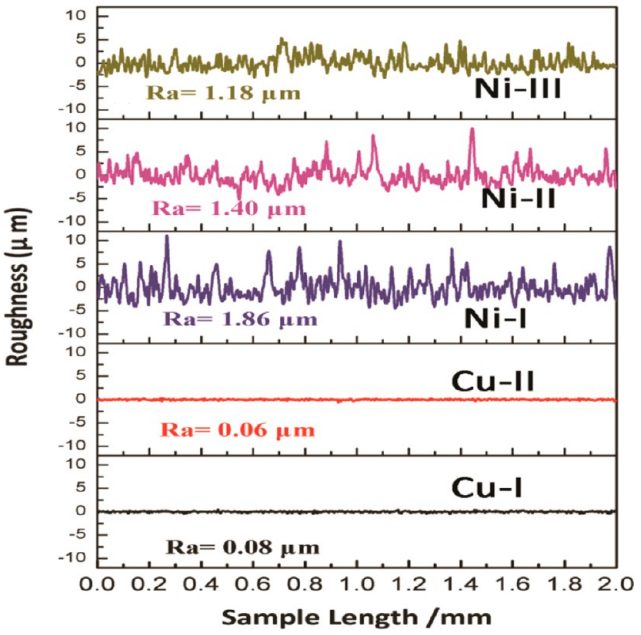

Figure 3. Surface roughness profile curves of various samples.

FTIR spectra of AC-FAS and the superhydrophobic surface are shown in Figure 4. A broad band at 1000-1130 cm^{-1}

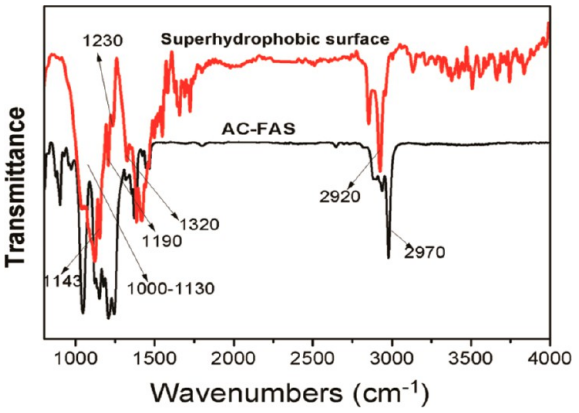

Figure 4. FTIR spectra of AC-FAS and the superhydrophobic surface.

resulting from the stretching of Si−O−Si are found for the superhydrophobic surface. The peaks at 1320, 1230, 1190, and 1145 cm^{-1} that are assigned to the C−F stretching vibration of the $-CF_3$ and $-CF_2$ groups from the AC-FAS molecules are observed on the superhydrophobic surface. The peak at 2970 cm^{-1}, which is attributed to the methyl symmetric stretching from AC-FAS, is not observed in the superhydrophobic surface. These results confirm that AC-FAS molecules have been successfully assembled on the surface of deposited Ni surface by heat treatment. To further confirm the self-assembly of the AC-FAS film on the Ni surface by heat treatment, Figure 5 displays the XPS spectra of the superhydrophobic surface. It can be seen that the superhydrophobic surface exhibits strong signals of F 1s, C 1s and O 1s and a weak signal of Si 2p. Figure 5f gives the XPS high-resolution of C 1s. The C 1s peaks locating at 292.5 and 289.8 eV are assigned to the carbon atom of $-CF_3$ and $-CF_2-$, respectively. The peak at 283.5 eV is assigned to the

dx.doi.org/10.1021/am501539b | ACS Appl. Mater. Interfaces 2014, 6, 8762−8770

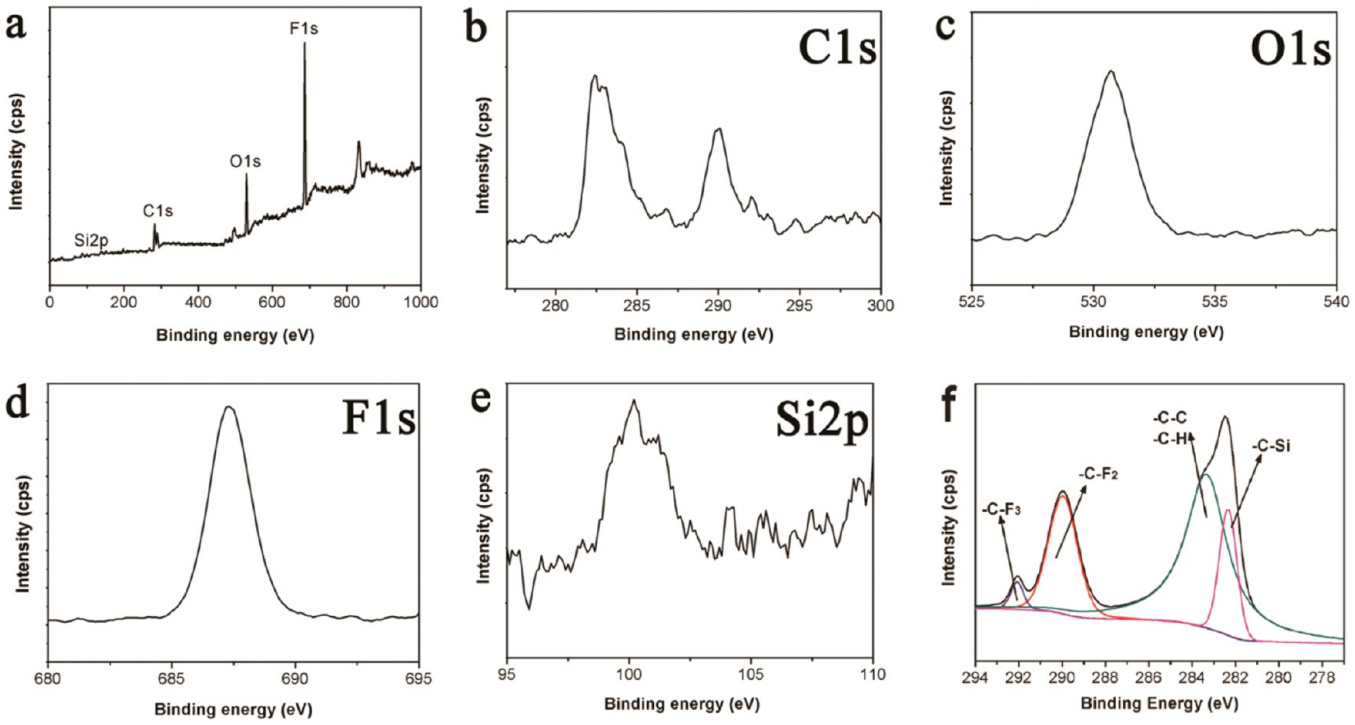

Figure 5. XPS spectra of the superhydrophobic surface: (a) XPS survey spectra, (b) C 1s, (c) O 1s, (d) F 1s, (e) Si 2p, and (f) high-resolution of C 1s.

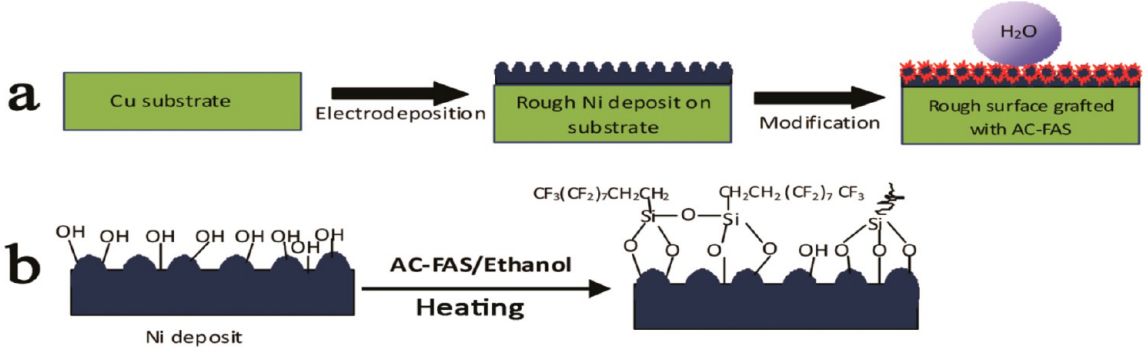

Figure 6. (a) Morphology evoluation of the surface deposited with Ni and then heated at 110 °C for 1 in the presence of AC-FAS. (b) Formation mechanism of the self-assembled AC-FAS film on the rough Ni surface.

carbon atom of −C−C and −C−H. The peak at 282.0 eV is attributed to the carbon atom of −C−Si.[31] These results further imply that the AC-FAS have successfully assembled on the surface of the deposited Ni surface by heat-treatment.

From these results obtained from Figures 2−5, it is clear that the superhydrophobic surface derives from its special microstructure and chemical compositions. The morphology evaluation of the sample surface after electrodeposition and heat-treatment can be displayed as Figure 6a. A rough Ni coating was firstly deposited on the Cu substrate by electrodeposition. However, the rough Ni surface is characterized with large dendrites and cylindrical microparticles, which is unfavorable to form the superhydrophobic surface. After the heat-treatment in the presence of AC-FAS, the modified surface is changed to be the pine-cone-like hierarchical micro-nanostructures. The rough surface with hierarchical micro-nanostructures has been confirmed to favor the formation of the superhydrophobic surface.[20,32,33] However, the rough surface is a necessary but not sufficient condition to achieve superhydrophobicity for this surface. It is well known that the surface wettability is also governed by its chemical compositions besides the surface morphology. Both the FTIR and XPS measurements confirm that the AC-FAS is successfully assembled on the deposited Ni surface by heat-treatment. The formation mechanism of the self-assembled AC-FAS film on the rough Ni surface can be elaborated as Figure 6b. The AC-FAS molecules react with the −OH groups of the deposited Ni surface to form a self-assembled film on the surface with the help of heating. The assembled AC-FAS film can effectively reduce the free energy of the deposited surface due to the its $-CF_3$ group with a surface energy of 6.7 $mJ{\cdot}m^{-2}$ and $-CF_2-$ group with a surface energy of 18 $mJ{\cdot}m^{-2}$. To sum up, it can be concluded that the superhydrophobicity of the as-prepared surface derives from its rough surface with pine-cone-like hierarchical micro-nanostructures and the presence of low-surface-energy fluorinated components on it.

3.2. Mechanical Stability. The mechanical stabilities including hardness and mechanical abrasion resistance are

Table 1. Comparisons of Hardness for Various Samples

sample	Cu-I	Cu-II	Ni-I	Ni-II	Ni-III
hardness (kgf mm^{-2})	230 ± 10	224 ± 10	416 ± 15	528 ± 18	385 ± 10
pencil hardness			>6H	>6H	>6H

very important for the practical application of the superhydrophobic surfaces. In this work, the microhardness test, pencil hardness test, and scratch test were performed to evaluate the mechanical stability of the as-prepared superhydrophobic surface. Comparisons of the hardness for various samples are shown in Table 1. It is clear the deposited Ni surface displays a microhardness of 416 ± 15 kgf·mm^{-2}, which is much higher than the bare Cu of 230 ± 10 kgf·mm^{-2}. After heat treatment, the microhardness increased to 528 ± 18 kgf·mm^{-2}. However, as the AC-FAS was used during the heating process, the microhardness of the as-prepared superhydrophobic decrease to 385 ± 10 kgf·mm^{-2}, which might be attributed to the self-assembled AC-FAS film on this coating. Compared to the bare Cu substrate, the superhydrophobic surface still exhibits much higher microhardness. In addition, the hardness of these surfaces has been evaluated by standard pencil hardness tests. The results show that the coating of Ni-I, Ni-II, and Ni-III display much higher hardness than 6H. The results mean that not only superhydrophobicity but high hardness are obtained for the sample surfaces constructed by electrodeposition and modification process. The high hardness can extend the applied range of the superhydrophobic materials.

Scratch tests were reported to be an effective method to evaluate the mechanical abrasion resistance of the superhydrophobic surfaces.[3,20,26] In this work, the similar scratch tests were carried out using 800 grit SiC sandpaper as an abrasion surface, as shown in Figure 7a. The superhydrophobic surfaces facing the abrasion material were tested at a speed of 4-5 mm·s^{-1} and varied applied pressure and sliding distance. Figure 7b shows that the surface still has superhydrophobicity with a contact angle of 157° and a sliding angle of 9.0° after abrasion for 1.0 m at 2.4 kPa. Figure 7b displays that the contact angle decreases and the sliding angle increases with the increase of applied pressure. After abrasion for 1.0 m at applied pressure of 4.8 kPa, the surface still has superhydrophobicity with a contact angle above 150°. When the applied pressure increases to 6.0 kPa, the contact angle decreases to 148° and the sliding angle increases to 31°. These results display that the as-prepared superhydrophobic surface has excellent mechanical abrasion resistance. It is much better than other reported superhydrophobic surfaces.[3,20,26] The superhydrophobic surface on magnesium alloy cannot endure the abrasion distance over 0.7 m at the applied pressure of 1.2 kPa.[3] The superhydrophobic surface formed on Si surfaces can only endure a pressure of 3.45 kPa after abrasion for 2.0 m.[26]

Figure 8 displays the SEM images of the resulting superhydrophobic surfaces after abrasion for 1.0 m at applied pressure of 2.4 and 6.0 kPa. SEM image of the superhydrophobic surface before abrasion is also shown in Figure 8a for reference. As shown in Figure 8b, a few shallow scratches are observed on the superhydrophobic surface after abrasion for 1.0 m at the pressure of 2.4 kPa, which suggests that the surface is slightly scratched by the hard sandpaper. As a result, the surface remains superhydrophobicity (see inserted figure). As the applied pressure of 6.0 kPa was used, the superhydrophobic surface is featured with severe abrasion wear, as shown in Figure 8c. It seems that a few microparticles with pine-cone-like structure have been destroyed and the new surface is generated. Because of the loss of the pine-cone-like hierarchical structures and the new surface exposed on the surface, the contact angles of this surface decrease and the sliding angles increase (Figure 7c).

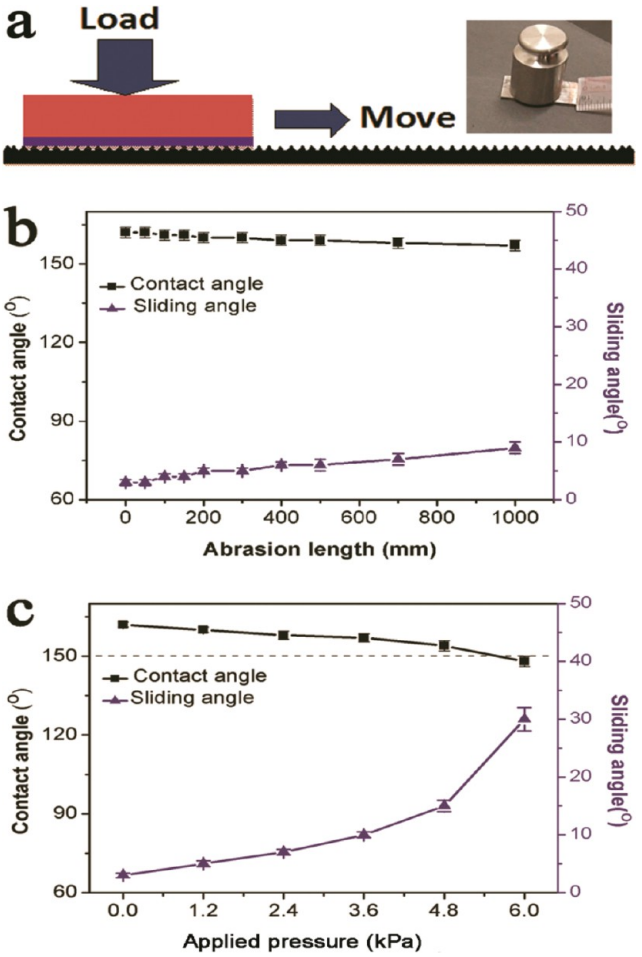

Figure 7. (a) Schematic illustration of the scratch test. (b) Contact angle and sliding angle of the superhydrophobic surfaces with increasing abrasion length at the applied pressure of 2.4 kPa. (c) Contact angle and sliding angle of the superhydrophobic surface with increasing applied pressure after abrasion for 1.0 m.

3.3. Chemical Stability and Corrosion Resistance. The superhydrophobic surfaces are always used in various corrosive environments and for a long time. Figure 9a show variations of the contact angles and sliding angles for the superhydrophobic surface as functions of pH value of water droplet. The pH value of the water droplet was adjusted by sulfuric acid and sodium hydroxide. It is clear that the as-prepared surface retains superhydrophobicity in pH values ranging from 1.0 to 13.0 because of their contact angles greater than 150° and sliding angle less than 10°. It suggests that the as-prepared superhydrophobic surface has good chemical stability in both acidic and alkaline environments. Figure 9b displays the change of the

dx.doi.org/10.1021/am501539b | ACS Appl. Mater. Interfaces 2014, 6, 8762−8770

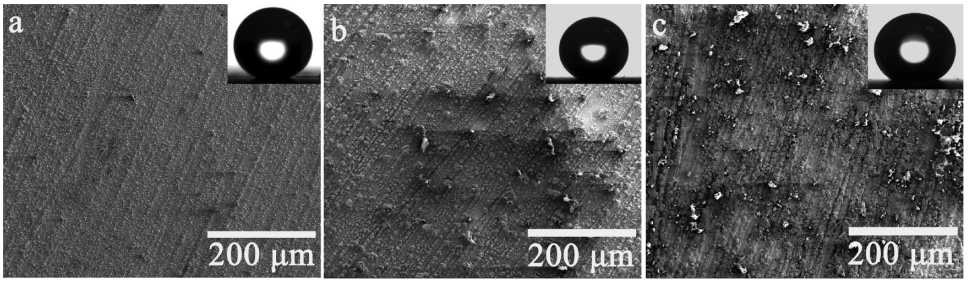

Figure 8. SEM images for the superhydrophobic surface before (a) and after abrasion for 1.0 m at applied pressure of 2.4 (b) and 6.0 kPa (c). Inset: Images of water droplet on the surface.

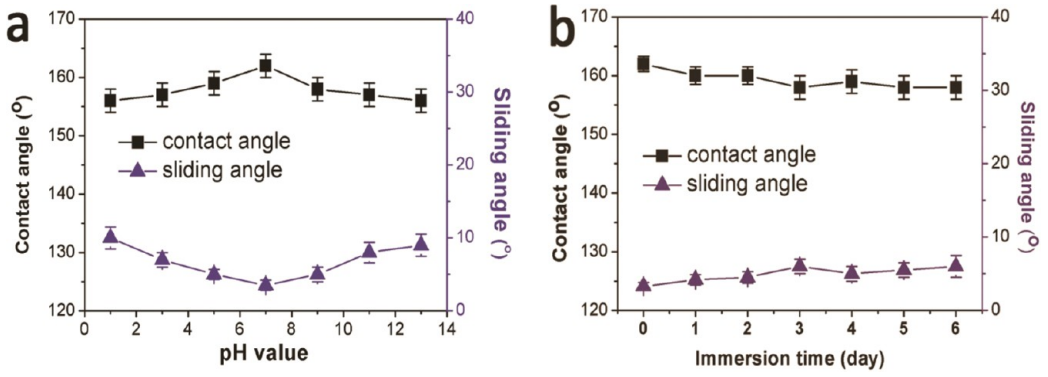

Figure 9. Influence of pH values of a wate droplet (a) and immersion time in water (b) on the contact angle and sliding angle of the superhydrophobic surfaces.

contact angles and sliding angles of the superhydrophobic surface as a function of the immersion time in water. The contact angle is slightly decreased to 158° from 162° and the sliding angle is slightly increased to 6.0° from 3.0° as the superhydrophobic surface was immersed in water for 6 days. This result suggests that the immersion in water does not greatly affect the surface states from the wettability point of view. That is to say, the as-prepared surface can maintain superhydrophobicity as it was immersed in water for several days.

The potentiodynamic polarization curves of the bare Cu substrate (Cu−I), electrodeposited Ni (Ni−I) and superhydrophobic surface (Ni-III) measured in 3.5 wt % NaCl solution are shown in Figure 10. The corrosion potential (E_{corr}), corrosion current density (i_{corr}) and corrosion rate using the Tafel extrapolation from the potentiodynamic polarization curves are given in Table 2. It can be seen that the electrodeposited Ni coating shows better corrosion resistance than the bare Cu substrate due to its lower corrosion current density and corrosion rate. As expected, the superhydrophobic surface has much better corrosion resistance than the bare Cu and deposited Ni coating. The corrosion current density of the superhydrophobic surface is approximately 1.4% that of the bare Cu and 9.2% that of the electrodeposited Ni coating. The superhydrophobic surface exhibits very low corrosion rate, a staggering 133-fold decrease from the bare Cu and 11-fold decrease from the unmodified Ni deposit. It can be concluded that the as-prepared superhydrophobic surface possesses a good anticorrosion protection for the bare Cu substrate.

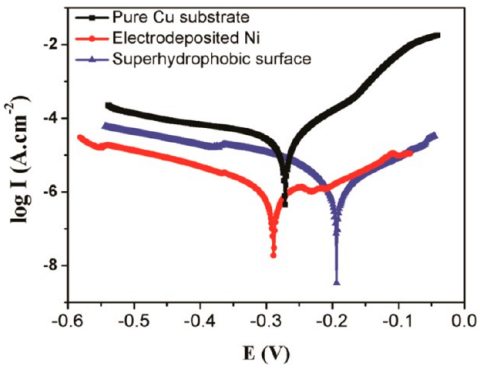

Figure 10. Potentiodynamic polarizaiton curves measured in 3.5 wt % NaCl solution for the bare Cu substrate (Cu-I), electrodeposited Ni (Ni-I), and superhydrohobic surface (Ni-III).

Table 2. Corrosion Potential (E_{corr}), Corrosion Current (i_{corr}), and Corrosion Rate of the Bare Cu, Deposited Ni, and Superhydrophobic Surface

sample	E_{corr} (mV)	I_{corr} (A cm^{-2})	corrosion rate (mm a^{-1})
bare Cu substrate	−271.4	2.72×10^{-5}	5.99×10^{-1}
electrodeposited Ni	−288.7	4.15×10^{-6}	4.88×10^{-2}
superhydrophobic surface	−222.4	3.83×10^{-7}	4.51×10^{-3}

EIS is one of the most efficient and intensively used methods for investigation and prediction of corrosion protection.[13,34] Figure 11 shows the Nyquist plots and Bode plots recorded for the bare Cu, electrodeposited Ni and the as-prepared superhydrophobic surface in 3.5 wt % NaCl solution. The diameter of the capacitive loop in the Nyquist plots represents the polarization resistance of the work electrode. As shown in Figure 11a, the superhydrophobic surface has the highest impedance value around 2.0×10^5 Ω·cm^{-2} that is 75 times

dx.doi.org/10.1021/am501539b | ACS Appl. Mater. Interfaces 2014, 6, 8762−8770

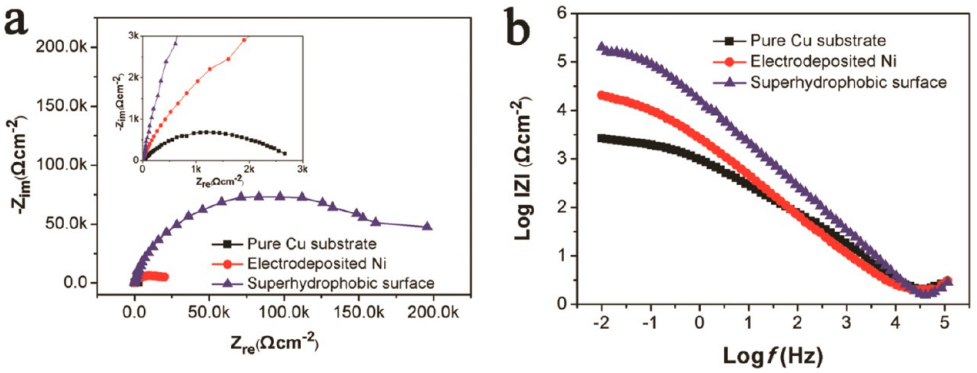

Figure 11. Nyquist plots (a) and Bode plots (b) of the bare Cu substrate, electrodeposited Ni surface, and the as-prepared superhydrophobic surface in 3.5 wt % NaCl solution.

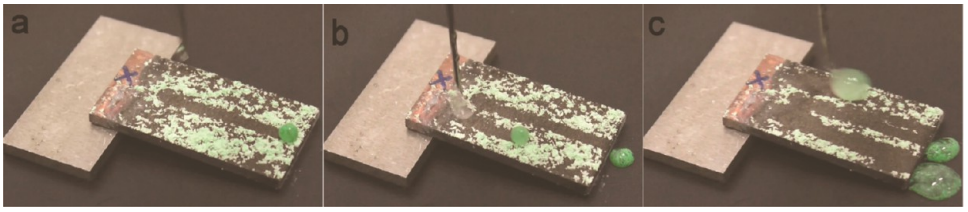

Figure 12. Evolution process of self-cleaning behavior of the as-prepared superhydrophobic surface.

higher than that of the bare Cu substrate and 10 times higher than that of the deposited Ni coating. Figure 11b presents the Bode plots (impedance modulus |Z| as a function of frequency) of the three samples in 3.5 wt % NaCl solution. It is clear that the superhydrophobic surface possesses the highest impedance modulus at low frequency, followed by the deposited Ni coating. These results from Figure 11 further confirm the as-prepared superhydrophobic surface provides excellent corrosion protection for the bare Cu substrate.

As illustrated above, the pine-cone-like hierarchical micro-nanostructure is necessary to achieve the superhydrophobicity for the as-prepared surface in this work. The hierarchical micro-nanostructures can generate numerous grooves in which the air can be trapped according to the Cassie–Baxter equation.[13,29] Because of the trapped air, the water drop from the corrosive medium might be suspended on the superhydrophobic surface. To confirm that, the as-prepared superhydrophobic surface was immersed in 3.5 wt % NaCl solution in this work (Video 2). It is clear that the superhydrophobic surface is completely nonstick to the corrosive water when it was immersed in and then taken out from 3.5 wt % NaCl solution. This result suggests that the air is indeed trapped in groove of surface and the liquid forms a convex surface between the interface of liquid and air for the capillary. The trapped air can effectively prevent corrosive media to penetrate into the surface and generate the better corrosion protection effect.[3,13]

3.4. Self-Cleaning Effect. It is important for superhydrophobic surfaces with self-cleaning ability for their practical applications. The self-cleaning effect of the as-prepared superhydrophobic surface is also investigated by applying chalk dust as contaminants to the surface. Figure 12 displays the evolution process of self-cleaning effect. It is clear the spherical water droplet began to roll quickly and remove the chalk dust, which might result from the joint action of high capillary forces induced by water droplet and the weak adhesion of the dusk particle to the superhydrophobic surface. The self-cleaning process (Video 3) depicts that the dusted surface become clean after the water droplet was free of the surface. Therefore, it can be concluded that the superhydrophobic surface can protect substrates from pollution in practical applications.

4. CONCLUSIONS

The mechanical abrasion resistance, corrosion resistance, and self-cleaning ability are of great importance for superhydrophobic surface applications. In this work, a superhydrophobic surface with a contact angle around 162° and a sliding angle around 3° is successfully constructed on the Cu substrate by a facile method. The superhydrophobicity of the constructed surface derives from its rough surface with pine-cone-like hierarchical micro-nanostructures and the assembly of low-surface-energy fluorinated components on it. The as-prepared superhydrophobic surface has high hardness, excellent mechanical abrasion resistance, and excellent corrosion resistance as well as self-cleaning ability. It can be used in both acidic and alkaline environments. The fabrication process containing electrodeposition and heat-treatment is very facile and low-cost, which offer an effective strategy and promising industrial applications for fabricating superhydrophobic surfaces on various metallic materials.

■ ASSOCIATED CONTENT

Ⓦ Web-Enhanced Features

Videos of the bouncing behavior of water droplet on the superhydrophobic surface, nonstick behavior of the superhydrophobic surface to corrosive water, and self-cleaning process of the superhydrophobic surface are available in the HTML version of this paper.

■ AUTHOR INFORMATION

Corresponding Author

*Fax: +86 2087112341. Tel: +86 2087112341. E-mail: fhsu@scut.edu.cn.

Notes

The authors declare no competing financial interest.

■ ACKNOWLEDGMENTS

The authors are grateful to the support of the National Natural Science Foundation of China (Grants 51275176), the Fundamental Research Funds for the Central Universities (Grants 2014ZG0014), and Pearl River Science & Technology Star (Grants: 2012J2200068) for financial support.

■ REFERENCES

(1) Wang, Z.; Li, Q.; She, Z.; Chen, F.; Li, L. Low-Cost and Large-Scale Fabrication Method for an Environmentally-Friendly Superhydrophobic Coating on Magnesium Alloy. *J. Mater. Chem.* **2012**, *22*, 4097−4105.

(2) Isimjan, T. T.; Wang, T.; Rohani, S. A Novel Method to Prepare Superhydrophobic, UV Resistance and Anti-corrosion Steel Surface. *Chem. Eng. J.* **2012**, *210*, 182−187.

(3) She, Z.; Li, Q.; Wang, Z.; Li, L.; Chen, F.; Zhou, J. Researching the Fabrication of Anticorrosion Superhydrophobic Surface on Magnesium Alloy and its Mechanical Stability and Durability. *Chem. Eng. J.* **2013**, *228*, 415−424.

(4) Jung, S.; Dorrestijn, M.; Raps, D.; Das, A.; Megaridis, C. M.; Poulikakos, D. Are Superhydrophobic Surfaces Best for Icephobicity? *Langmuir* **2011**, *27*, 3059−3066.

(5) Wang, C.; Yao, T.; Wu, J.; Ma, C.; Fan, Z.; Wang, Z.; Cheng, Y.; Lin, Q.; Yang, B. Facile Approach in Fabricating Superhydrophobic and Superoleophilic Surface for Water and Oil mixture Separation. *ACS Appl. Mater. Interfaces* **2009**, *1*, 2613−2617.

(6) Li, J.; Shi, L.; Chen, Y.; Zhang, Y.; Guo, Z.; Su, B.-l.; Liu, W. Stable Superhydrophobic Coatings from Thiol-ligand Nanocrystals and their Application in Oil/Water Separation. *J. Mater. Chem.* **2012**, *22*, 9774−9781.

(7) Sousa, M. P.; Mano, J. F. Patterned Superhydrophobic Paper for Microfluidic Devices Obtained by Writing and Printing. *Cellulose.* **2013**, *20*, 2185−2190.

(8) Kim, H.; Noh, K.; Choi, C.; Khamwannah, J.; Villwock, D.; Jin, S. Extreme Superomniphobicity of Multiwalled 8 nm TiO_2 Nanotubes. *Langmuir* **2011**, *27*, 10191−10196.

(9) Xu, L.; Karunakaran, R. G.; Guo, J.; Yang, S. Transparent, Superhydrophobic Surfaces from One-Step Spin Coating of Hydrophobic Nanoparticles. *ACS Appl. Mater. Interfaces* **2012**, *4*, 1118−1125.

(10) Chen, Z.; Hao, L.; Chen, A.; Song, Q.; Chen, C. A Rapid One-Step Process for Fabrication of Superhydrophobic Surface by Electrodeposition Method. *Electrochim. Acta* **2012**, *59*, 168−171.

(11) Yao, X.; Xu, L.; Jiang, L. Fabrication and Characterization of Superhydrophobic Surfaces with Dynamic Stability. *Adv. Funct. Mater.* **2010**, *20*, 3343−3349.

(12) Zhu, X.; Zhang, Z.; Xu, X.; Men, X.; Yang, J.; Zhou, X.; Xue, Q. Facile Fabrication of a Superamphiphobic Surface on the Copper Substrate. *J. Colloid Interface Sci.* **2012**, *367*, 443−439.

(13) She, Z.; Li, Q.; Wang, Z.; Li, L.; Chen, F.; Zhou, J. Novel Method for Controllable Fabrication of a Superhydrophobic CuO Surface on AZ91D Magnesium Alloy. *ACS Appl. Mater. Interfaces* **2012**, *4*, 4348−4356.

(14) Yu, J.; Qin, L.; Hao, Y.; Kuang, S.; Bai, X.; Chong, Y.-M.; Zhang, W.; Wang, E. Vertically Aligned Boron Nitride Nanosheets: Chemical Vapor Synthesis,Ultraviolet Light emission, and Superhydrophobicity. *ACS Nano* **2010**, *4*, 414−422.

(15) Qian, B.; Shen, Z. Fabrication of Superhydrophobic Surfaces by Dislocation-Selective Chemical Etching on Aluminum, Copper, and Zinc substrates. *Langmuir* **2005**, *21*, 9007−9009.

(16) Rao, A. V.; Latthe, S. S.; Mahadik, S. A.; Kappenstein, C. Mechanically Stable and Corrosion Resistant Superhydrophobic Sol−Gel Coatings on Copper Substrate. *Appl. Surf. Sci.* **2011**, *257*, 5772−5776.

(17) Chaudhary, A.; Barshilia, H. C. Nanometric Multiscale Rough $CuO/Cu(OH)_2$ Superhydrophobic Surfaces Prepared by a Facile One-Step Solution-Immersion Process: Transition to Superhydrophilicity with Oxygen Plasma Treatment. *J. Phys. Chem. C* **2011**, *115*, 18213−18220.

(18) Dong, C.; Gu, Y.; Zhong, M.; Li, L.; Sezer, K.; Ma, M.; Liu, W. Fabrication of Superhydrophobic Cu Surfaces with Tunable Regular Micro and Random Nano-scale Structures by Hybrid Laser Texture and Chemical Etching. *J. Mater. Process.Technol.* **2011**, *211*, 1234−1240.

(19) Su, F.; Yao, K.; Liu, C.; Huang, P. Rapid Fabrication of Corrosion Resistant and Superhydrophobic Cobalt Coating by a One-Step Electrodeposition. *J. Electrochem. Soc.* **2013**, *160*, D593−D599.

(20) Zhu, X.; Zhang, Z.; Men, X.; Yang, J.; Wang, K.; Xu, X.; Zhou, X.; Xue, Q. Robust Superhydrophobic Surfaces with Mechanical Durability and Easy Repairability. *J. Mater. Chem.* **2011**, *21*, 15793−15797.

(21) Zhu, X.; Zhang, Z.; Yang, J.; Xu, X.; Men, X.; Zhou, X. Facile Fabrication of a Superhydrophobic Fabric with Mechanical Stability and Easy-Repairability. *J. Colloid Interface Sci.* **2012**, *380*, 182−186.

(22) Lee, S.-M.; Kim, K.-S.; Pippel, E.; Kim, S.; Kim, J.-H.; Lee, H.-J. Facile Route Toward Mechanically Stable Superhydrophobic Copper Using Oxidation−Reduction Induced Morphology Changes. *J. Phys. Chem. C* **2012**, *116*, 2781−2790.

(23) Boinovich, L.; Emelyanenko, A. A Wetting Experiment as a Tool to Study the Physicochemical Processes Accompanying the Contact of Hydrophobic and Superhydrophobic Materials with Aqueous Media. *Adv. Colloid Interface Sci.* **2012**, *179*, 133−141.

(24) Ishizaki, T.; Saito, N. Rapid Formation of a Superhydrophobic Surface on a Magnesium Alloy Coated with a Cerium Oxide Film by a Simple Immersion Process at Room Temperature and Its Chemical Stability. *Langmuir* **2010**, *26*, 9749−9755.

(25) Guo, F.; Su, X.; Hou, G.; Li, P. Bioinspired Fabrication of Stable and Robust Superhydrophobic Steel Surface with Hierarchical Flowerlike Structure. *Colloids Surf., A* **2012**, *401*, 61−67.

(26) Xiu, Y.; Liu, Y.; Hess, D. W.; Wong, C. Mechanically Robust Duperhydrophobicity on Hierarchically Structured Si Surfaces. *Nanotechnology* **2010**, *21*, 155705.

(27) Liu, T.; Yin, Y.; Chen, S.; Chang, X.; Cheng, S. Super-Hydrophobic Surfaces Improve Corrosion Resistance of Copper in Seawater. *Electrochim. Acta* **2007**, *52*, 3709−3713.

(28) Yuan, S.; Pehkonen, S.; Liang, B.; Ting, Y.; Neoh, K.; Kang, E. Superhydrophobic Fluoropolymer-Modified Copper Surface via Surface Graft Polymerisation for Corrosion Protection. *Corros. Sci.* **2011**, *53*, 2738−2747.

(29) Cassie, A.; Baxter, S. Wettability of Porous Surfaces. *Trans. Faraday Soc.* **1944**, *40*, 546−551.

(30) Erbil, H. Y.; Cansoy, C. E. Range of Applicability of the Wenzel and Cassie−Baxter Equations for Superhydrophobic Surfaces. *Langmuir* **2009**, *25*, 14135−14145.

(31) Saleema, N.; Sarkar, D. K.; Paynter, R. W.; Chen, X. G. Superhydrophobic Aluminum Alloy Surfaces by a Novel One-Step Process. *ACS Appl. Mater. Interfaces* **2010**, *2*, 2500−2502.

(32) Liu, K.; Zhang, M.; Zhai, J.; Wang, J.; Jiang, L. Bioinspired Construction of Mg−Li Alloys Surfaces with Stable Superhydrophobicity and Improved Corrosion Resistance. *Appl. Phys. Lett.* **2008**, *92*, No. 183103.

(33) Xu, W.; Song, J.; Sun, J.; Lu, Y.; Yu, Z. Rapid Fabrication of Large-area, Corrosion-Resistant Superhydrophobic Mg Alloy Surfaces. *ACS Appl. Mater. Interfaces* **2011**, *3*, 4404−4414.

(34) Zhang, S.; Li, Q.; Chen, B.; Yang, X. Preparation and Corrosion Resistance Studies of Nanometric Sol−Gel-Based CeO_2 Film with a Chromium-Free Pretreatment on AZ91D magnesium alloy. *Electrochim. Acta* **2010**, *55*, 870−877.